A Spectral Integral Method (SIM) for Layered Media

Ergün Şimşek, *Student Member, IEEE*, Jianguo Liu, *Student Member, IEEE*, and Qing Huo Liu, *Fellow, IEEE*

***Abstract*—A spectral integral method is presented for electromagnetic scattering from dielectric and perfectly electric conducting (PEC) objects with a closed boundary embedded in a layered medium. Two-dimensional layered medium Green's functions are computed adaptively by using Gaussian quadratures. The singular terms in the Green's functions and the non-smooth terms in their derivatives are handled appropriately to achieve exponential convergence. Numerical results, compared with the ones obtained by using other methods, demonstrate the spectral accuracy and high efficiency of the proposed method. They also confirm that the spectral integral method (SIM) is applicable to concave objects.**

***Index Terms*—Boundary integral method, Green's functions, layered media, spectral integral method (SIM).**

I. Introduction

FOR a homogeneous scatterer with an arbitrary geometry in a layered medium, the surface integral equation method is a powerful tool to calculate the scattered electromagnetic fields. The classical methods for solving such integral equations are the method of moments (MOM) [1]–[5], fast multipole method (FMM) [6]–[10], and adaptive integral method [11]–[16].

Recently, Liu *et al.* [17] proposed a spectral integral method as an alternative way of solving the surface integral equation efficiently for a homogeneous scatter in free space and for periodic structures. This algorithm is related to the fast method originally developed by Bojarski [18] for sound-soft circular cylinders, and extended by Schuster [19] to multilayer circular cylinders, and by Hu [20] to sound-soft or sound-hard smooth cylinders. Liu *et al.* [17] further extended the SIM to arbitrarily-shaped smooth dielectric cylinders, and to periodic structures such as photonic crystals. The idea behind this method is the use of fast Fourier transform (FFT) algorithm and the subtraction of singularities in Green's functions to achieve a spectral accuracy in the integral. Here, we extend this method to arbitrarily-shaped smooth dielectric and PEC cylinders embedded in layered media by using two-dimensional (2-D) layered-medium Green's functions. To avoid the discontinuous behaviors of the fields and Green's function (i.e., the functions or their derivatives being discontinuous) across the layer interfaces in the problems where the scatterer resides in several layers, in this work the object must locate completely within one single layer in the multilayered medium. Future research will investigate objects traversing several layers where such discontinuities must be properly treated.

Manuscript received April 4, 2005; revised January 10, 2006. This work was supported by the National Science Foundation under Grants CCR-00-98140 and IIS-0086075.

The authors are with the Department of Electrical and Computer Engineering, Duke University, Durham, NC 27708-0291 USA (e-mail: qhliu@ee.duke.edu).

Digital Object Identifier 10.1109/TAP.2006.875500

The outline of this paper is as follows: first the brief formulation of 2-D layered-medium Green's function is presented. Next, the implementation of SIM for layered media is described. Finally, the accuracy and the efficiency of the method are verified with several numerical examples. This method can also be extended to periodic structures [17]. The potential extension to three dimensions (3-D) is under investigation.

II. 2-D Green's Functions

Consider a general multilayer medium consisting of N layers separated by $N-1$ interfaces parallel to the x axis. Layer i $(i=1,\cdots,N)$ exists between $y=y_i$ and y_{i-1} ($y_0 \to -\infty$ and $y_N \to \infty$) and is characterized by relative complex permittivity $\tilde{\epsilon}_{r,i}$ and relative permeability $\mu_{r,i}$, the wavenumber inside the layer is given by $k_i=\omega\sqrt{\tilde{\epsilon}_i\mu_i}$. The time dependency of e^{jwt} is implied.

In the absence of a scatterer, the electric or magnetic field at (x,y) due to a unit line source at (x',y') can be calculated by using layered-medium Green's functions. The formulation of the Green's function for 2-D is very similar to the 3-D case, and the reader may refer to [1], [21], [22], and [28] for the details of derivation. Essentially, by transforming the problem from the spatial domain to spectral domain, each layer can be represented by a uniform transmission line having the same physical properties; hence the electric and magnetic fields can be interpreted as voltage and current, respectively, on a transmission line. By using this transmission line analogy, Green's functions in the spectral domain, called transmission line Green's functions (TLGF), can be derived easily. The spatial domain Green's function is the inverse transformation from spectral domain to spatial domain and is known as a Sommerfeld integral given by

$$G^p(x-x',y|y')=\frac{1}{\pi}\int_0^\infty \tilde{\tilde{G}}^p_{mn}(k_x,y|y')\cos k_x(x-x')dk_x \quad (1)$$

where $G^p(x-x',y|y')$ is the p type (p is either TE_z or TM_z) Green's function relating the field at (x,y) in layer m due to a unit source at (x',y') in layer n; $\tilde{\tilde{G}}^p_{mn}$ is its spectral domain counterpart (TLGF) which has a closed form expression depending on the locations of the source and field points

$$\tilde{\tilde{G}}^p=\frac{\tilde{G}^p_{mn}}{j\omega\varsigma^p_m} \quad (2)$$

the subscripts mn refer to the source layer (n) and field layer (m), and ς^p_n is either μ_m or $\tilde{\epsilon}_m$ for TE_z or TM_z cases, respectively.

A. $m = n$

When the source and field points belong to the same layer

$$\tilde{G}^p_{nn}(y|y') = \frac{\omega\varsigma^p_n}{2k_{y,n}}\left(A^p_0 + A^p_{1,2,3,4}/D^p_n\right). \tag{3}$$

In the above, $A_{i,\cdots,k} = A_i + \cdots + A_k$

$$\begin{aligned} A^p_i &= a^p_i e^{-jk_{y,n}\alpha_i}, \quad i = 0,1,2,3,4 && (4)\\ \alpha_0 &= |y - y'| && a^p_0 = 1\\ \alpha_1 &= 2y_n - (y + y') && a^p_1 = \Gamma^p_{n,n+1}\\ \alpha_2 &= (y + y') - 2y_{n-1} && a^p_2 = \Gamma^p_{n,n-1}\\ \alpha_3 &= 2d_n + (y - y') && a^p_3 = a^p_1 a^p_2\\ \alpha_4 &= 2d_n - (y - y') && a^p_4 = a^p_3\\ D^p_n &= 1 - a^p_3 e^{-j2k_{y,n}d_n} && (5) \end{aligned}$$

where $\Gamma^p_{i,j}$ is the p type generalized reflection coefficient which can be calculated recursively by [21]

$$\Gamma^p_{i,i+1} = \frac{R^p_{i,i+1} + \Gamma^p_{i+1,i+2}e^{-j2k_{y,i+1}d_{i+1}}}{1 + R^p_{i,i+1}\Gamma^p_{i+1,i+2}e^{-j2k_{y,i+1}d_{i+1}}} \tag{6}$$

where d_i is the thickness of ith layer, $k_{y,i} = \sqrt{k_i^2 - k_x^2}$, and $R^p_{i,i+1}$ denotes the p type Fresnel reflection coefficient given by

$$R^p_{i,i+1} = \frac{\varsigma^p_{i+1}k_{y,i} - \varsigma^p_i k_{y,i+1}}{\varsigma^p_{i+1}k_{y,i} + \varsigma^p_i k_{y,i+1}}. \tag{7}$$

Note that,

$$\lim_{k_x\to\infty} k_{y,i} = k_{y,j} = -jk_x \tag{8}$$

$$\lim_{k_x\to\infty} \Gamma^p_{i,j} = \frac{\varsigma^p_j - \varsigma^p_i}{\varsigma^p_j + \varsigma^p_i}. \tag{9}$$

This means that A^p_i terms may converge to a number which is different than 0. The subtraction of integrand's asymptote increases its decaying speed. $\tilde{G}^{p,(0)}_{nn}(y|y')$, the asymptote of $\tilde{G}^p_{nn}(y|y')$, can be given as

$$\tilde{G}^{p,(0)}_{nn}(y|y') = \frac{\omega\varsigma^p_n}{2k_{y,n}}B^p_{0,1,2,3,4} \tag{10}$$

$$B^p_i = b^p_i e^{-jk_{y,n}\alpha_i}, \quad i = 0,1,2,3,4 \tag{11}$$

$$\begin{aligned} b^p_0 &= 1, \quad b^p_1 = R^p_{n,n+1},\\ b^p_2 &= R^p_{n,n-1}, \quad b^p_3 = b^p_4 = b^p_1 b^p_2 && (12) \end{aligned}$$

The subtracted terms' contribution in spatial domain can be written as

$$G^{p,(0)}(x - x', y|y') = \frac{1}{4j}\sum_{i=0}^{4} b^p_i H^{(2)}_0(k_m\rho_i) \tag{13}$$

where $\rho_i = \sqrt{(x - x')^2 + \alpha_i^2}$.

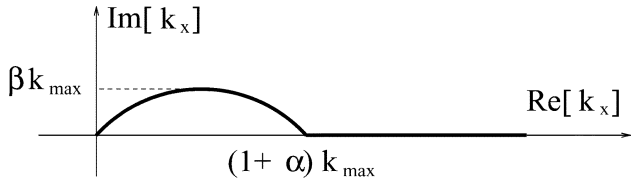

Fig. 1. Sommerfeld integration path in the complex k_x plane, where $k_{\max} = \max\{Re(k_1, k_2, \cdots, k_N)\}$, $\alpha > 0$, and $\beta > 0$. In the numerical examples, $\alpha = 0.2$ and $\beta = 0.001$ are used.

B. $m \neq n$

When the source and field points are in different layers and $m > n$, the spectral domain Green's function can be computed by using voltage/current transfer functions as follows:

$$\tilde{G}^p_{mn}(y|y') = T^p_{mm}T^p_{mn}\tilde{G}^p_{nn}(y_n|y') \tag{14}$$

where T^p_{mm} denotes the p type transfer function between a point y in layer m and the lower boundary of that layer, y_{m-1}; and T_{mn} denotes the p type transfer function between y_{m-1} and the upper boundary of the nth layer, y_n

$$T^p_{mm} = \frac{\left[1 + \Gamma^p_{m,m+1}e^{-j2k_{y,m}(y_m - y)}\right]e^{-jk_{y,m}(y - y_{m-1})}}{1 + \Gamma^p_{m,m+1}e^{-j2k_{y,m}d_m}} \tag{15}$$

$$T^p_{mn} = \prod_{t=n+1}^{m-1}\frac{\left(1 + \Gamma^p_{t,t+1}\right)e^{-jk_{y,t}d_t}}{1 + \Gamma^p_{t,t+1}e^{-j2k_{y,t}d_t}}. \tag{16}$$

Multiplication of these two terms with $\tilde{G}^p_{nn}(y_n|y')$ gives $\tilde{G}^p_{mn}(y|y')$. Note that $T^p_{mn} = 1$ when $m = n + 1$.

The formulation for $m < n$ is very similar to the case where $m > n$ and can be obtained easily by using symmetry.

For the 3-D case, it is shown that the efficiency of the numerical integration can be improved by deforming the integration path in the complex k_ρ plane [21], [23]. As shown in Fig. 1, the maximum displacement from the real axis is set to $\beta k_{\max}$. Since the first integration segment requires little computation time compared to the whole Sommerfeld integral, we have not optimized the choice of β. In the following numerical examples, we chose $\alpha = 0.2$ and $\beta = 0.001$. The reader is referred to [29] for more discussions on the integration path. By using the deformed Sommerfeld integration path depicted in Fig. 1, the spatial domain Green's functions can be calculated numerically. In this work, to speed up the numerical evaluation of the Sommerfeld integrals, we subtract the direct field term between the source and field points and the so-called "quasi-dynamic" term in the reflection (i.e., the term at the limit when $k_x \to \infty$) when $m = n$, and the "quasi-dynamic" transmission term when $m \neq n$. (One 3-D version of such subtraction is reported in [24].) The extraction of the quasi dynamic terms improves the convergence of the spectral integrals for the reflected field in the case where the source and the observation points are near the layer interfaces (i.e., when either α_1 or α_2 in (5) are small with respect to the minimum wavelength).

III. Spectral Integration Method for Layered Media

For the TM_z case, the 2-D Helmholtz equation for the scalar field E_z is

$$\nabla^2 E_z + k_\gamma^2 E_z = -f_\gamma \tag{17}$$

where subscript γ indicates the region outside ($\gamma = l$) or inside ($\gamma = d$) the object, f_γ is the source excitation, $k_l = \omega\sqrt{\mu_l \tilde{\epsilon}_l}$ for the lth layer ($l = 1, 2, \cdots, N$) and $k_d = \omega\sqrt{\mu_d \tilde{\epsilon}_d}$ for the dielectric object. Since the formulation and all the examples are presented here for the TM_z case, the superscript p is omitted for the rest of the formulation. In this work, we assume the scatterer is entirely within one layer.

For a smooth dielectric object embedded in a layered medium, the boundary integral equations on the surface of the scatterer D are

$$E_z^{\mathrm{inc}}(\mathbf{r}) + \oint_D \left[\frac{\partial E_z(\mathbf{r}')}{\partial n'} G_l(\mathbf{r}, \mathbf{r}') - E_z(\mathbf{r}') \frac{\partial G_l(\mathbf{r}, \mathbf{r}')}{\partial n'}\right] ds' = \frac{E_z(\mathbf{r})}{2} \tag{18}$$

$$- \oint_D \left[\frac{\partial E_z(\mathbf{r}')}{\partial n'} G_d(\mathbf{r}, \mathbf{r}') - E_z(\mathbf{r}') \frac{\partial G_d(\mathbf{r}, \mathbf{r}')}{\partial n'}\right] ds' = \frac{E_z(\mathbf{r})}{2} \tag{19}$$

for $\mathbf{r} \in D$, where f_d is assumed zero, E_z^{inc} is the incident wave from outside the object (i.e., $f_l \neq 0$, $f_d = 0$). $\hat{\mathbf{n}}$ is the outward unit normal, and $R = |\mathbf{r} - \mathbf{r}'|$. Inside the dielectric object, the homogeneous space Green's function and its normal derivative can be written as

$$G_d(\mathbf{r}, \mathbf{r}') = -\frac{j}{4} H_0^{(2)}(k_d R) \tag{20}$$

$$\frac{\partial G_d(\mathbf{r}, \mathbf{r}')}{\partial n'} = \frac{jk_d}{4} H_1^{(2)}(k_d R) \frac{\mathbf{R} \cdot \hat{\mathbf{n}}'}{R}. \tag{21}$$

Outside the object, the layered-medium Green's function is required and it can be written as a summation of two separate terms: the primary field term (G_{pri}) and the remaining reflection term (G_{refl}):

$$G(x - x', y|y') = G_{\mathrm{pri}} + G_{\mathrm{refl}} \tag{22}$$

Then its normal derivative can be written as

$$\frac{\partial G_l}{\partial n'} = \frac{\partial G_{\mathrm{pri}}}{\partial n'} + \frac{\partial G_{\mathrm{refl}}}{\partial n'} = \frac{\partial G_{\mathrm{pri}}}{\partial n'} + \hat{\mathbf{n}}' \cdot \nabla G_{\mathrm{refl}} = \frac{\partial G_{\mathrm{pri}}}{\partial n'} + \frac{\partial G_{\mathrm{refl}}}{\partial x'} \frac{\partial y'}{\partial \theta'} - \frac{\partial G_{\mathrm{refl}}}{\partial y'} \frac{\partial x'}{\partial \theta'} \tag{23}$$

where $(x' = x(\theta'), y' = y(\theta'))$ describe the surface of the scatterer. The primary field term G_{pri} and its derivative are the same as (21) except k_d should be replaced by k_l, and

$$\frac{\partial G_{\mathrm{refl}}}{\partial x'} = \frac{1}{\pi} \int_0^\infty \left[\tilde{G}_{\mathrm{refl}} - \tilde{G}_{\mathrm{refl}}^{(0)}\right] k_x \sin k_x (x - x') dk_x + g_1^{(0)}(x - x', y, y') \tag{24}$$

$$\frac{\partial G_{\mathrm{refl}}}{\partial y'} = \frac{1}{\pi} \int_0^\infty \left[\frac{\partial \tilde{G}_{\mathrm{refl}}}{\partial y'} - \frac{\partial \tilde{G}_{\mathrm{refl}}^{(0)}}{\partial y'}\right] \cos k_x (x - x') dk_x + g_2^{(0)}(x - x', y, y') \tag{25}$$

where

$$\frac{\partial \tilde{G}_{\mathrm{refl}}}{\partial y'} = \frac{j\omega\varsigma_l}{2D_l}\{A_{1,3} - A_{2,4}\} \tag{26}$$

$$\frac{\partial \tilde{G}_{\mathrm{refl}}^{(0)}}{\partial y'} = \frac{j\omega\varsigma_l}{2}\{B_{1,3} - B_{2,4}\} \tag{27}$$

$$g_1^{(0)}(x - x', y, y') = \frac{k_l}{4j} \sum_{i=1}^{4} b_i H_1^{(2)}(k_l \rho_i) \frac{(x - x')}{\rho_i} \tag{28}$$

$$g_2^{(0)}(x - x', y, y') = \frac{k_l}{4j} \sum_{i=1}^{4} b_i H_1^{(2)}(k_l \rho_i) \frac{(-1)^i \alpha_i}{\rho_i} \tag{29}$$

are the so-called "quasi-dynamic" terms. With such subtractions, the Sommerfeld integral can be calculated more rapidly.

With the above Green's functions and their derivatives, (18) can be rewritten in terms of a parameter θ along the boundary:

$$E_z^{\mathrm{inc}}(\theta) = \frac{E_z(\theta)}{2} - \int_0^{2\pi} \frac{\partial E_z(\theta')}{\partial n'} G_l(\theta, \theta') \left|\frac{d\mathbf{r}'}{d\theta'}\right| d\theta' + \int_0^{2\pi} E_z(\theta') \frac{\partial G_l(\theta, \theta')}{\partial n'} \left|\frac{d\mathbf{r}'}{d\theta'}\right| d\theta' \tag{30}$$

where $|d\mathbf{r}'/d\theta'| = ds'/d\theta' = \sqrt{(r')^2 + (dr'/d\theta')^2}$ and $r' = r(\theta')$. Since the scatterer has a smooth surface, and $E_z(\theta)$ and $\partial E_z(\theta)/\partial n$ are smooth and periodic functions of θ on the closed boundary, they can be approximated by truncated Fourier series as

$$E_z^N(\theta) = \sum_{n=-\frac{N}{2}}^{\frac{N}{2}-1} \phi_n e^{-jn\theta} \tag{31}$$

$$\frac{\partial E_z^N(\theta)}{\partial n'} = \sum_{n=-\frac{N}{2}}^{\frac{N}{2}-1} \psi_n e^{-jn\theta} \tag{32}$$

where ϕ_n and ψ_n are Fourier coefficients. By substituting them into (30), we have

$$E_z^{\text{inc}}(\theta) = \frac{1}{2}\sum_{n=-\frac{N}{2}}^{\frac{N}{2}-1}\phi_n e^{-jn\theta} - \sum_{n=-\frac{N}{2}}^{\frac{N}{2}-1}\psi_n \int_0^{2\pi} e^{-jn\theta'} G_l(\theta,\theta')\left|\frac{d\mathbf{r}'}{d\theta'}\right| d\theta' + \sum_{n=-\frac{N}{2}}^{\frac{N}{2}-1}\phi_n \int_0^{2\pi} e^{-jn\theta'} \frac{G_l(\theta,\theta')}{\partial n'}\left|\frac{d\mathbf{r}'}{d\theta'}\right| d\theta'. \quad (33)$$

The above integrals are simply Fourier transforms and can be calculated using FFT. However, to be able to obtain spectral accuracy, singular terms in the Green's functions and the non-smooth terms in their derivatives must be handled carefully. As described in [20], two infinitely smooth functions are defined as follows:

$$\hat{G}_\gamma(\theta,\theta') \equiv G_\gamma(\theta,\theta') + \frac{1}{2\pi}\ln\left|2\sin\left(\frac{\theta-\theta'}{2}\right)\right| \times J_0(k_\gamma R) \quad (34)$$

$$\hat{H}_\gamma(\theta,\theta') \equiv \frac{\partial G_\gamma(\theta,\theta')}{\partial n'} - \frac{k_\gamma}{2\pi}\ln\left|2\sin\left(\frac{\theta-\theta'}{2}\right)\right| \times J_1(k_\gamma R)\frac{\mathbf{R}\cdot\mathbf{n}}{R}. \quad (35)$$

In [17], the free space Green's functions are used. For our problem here, the layered-medium Green's functions must be used. Since the singularity occurs only for the primary field term when source and field points are in the same layer, one can add the layered-medium Green's function (without the primary field term) and its derivative directly to the smooth terms, $\hat{G}_\gamma(\theta,\theta')$ and $\hat{H}_\gamma(\theta,\theta')$, respectively. Uniformly sampled N points along the surface of the scatterer are used as testing points as in the point-matching (collocation) in MOM. After testing, (33) becomes

$$E_z^{\text{inc}}(\theta) = \sum_{n=-\frac{N}{2}}^{\frac{N}{2}-1}\phi_n\left(2\pi h_{l,mn} - k_0 v_{l,mn}\right) - \sum_{n=-\frac{N}{2}}^{\frac{N}{2}-1}\psi_n(2\pi g_{l,mn} - u_{l,mn}) + \frac{1}{2}\sum_{n=-\frac{N}{2}}^{\frac{N}{2}-1}\phi_n E_{mn} \quad (36)$$

where $E_{mn} = e^{in\theta_m}$; m is the index of a testing point on the boundary, and n the index of the Fourier series; $g_{l,mn}$ and $h_{l,mn}$ are Fourier transforms of the smooth part of the $G_l(\theta_m,\theta'_n)$ and $H_l(\theta_m,\theta'_n) = \partial G_l(\theta_m,\theta'_n)/\partial n'$, respectively; $u_{l,mn}$ and $v_{l,mn}$ are Fourier transforms of the non-smooth term of the $G_l(\theta_m,\theta'_n)$ and $H_l(\theta_m,\theta'_n)$, respectively, and can be calculated via convolution of the logarithmic functions with the Bessel functions [17], [20].

Equation (19) can be discretized in the same way. Then (36) and the equation corresponding to (19) can be written in a matrix form as follows:

$$\mathbf{C}^l\mathbf{\Phi} + \mathbf{D}^l\mathbf{\Psi} = \mathbf{F} \quad (37)$$

$$\mathbf{C}^d\mathbf{\Phi} + \mathbf{D}^d\mathbf{\Psi} = 0 \quad (38)$$

where $C^\gamma_{mn} = 2\pi h^\gamma_{mn} + k_\gamma v^\gamma_{mn} + (-1)^j E_{mn}/2$, $D^\gamma_{mn} = -2\pi g^\gamma_{mn} + u^\gamma_{mn}$, $F_m = E^{\text{inc}}_{z,m}$, $\mathbf{\Phi}$ and $\mathbf{\Psi}$ are vectors of ϕ_n and ψ_n, respectively.

By using (37) and (38), ϕ_n and ψ_n can be obtained easily. Then the scalar field (E_z) and its normal derivative ($\partial E_z/\partial n'$) on the boundary of the scatter can be computed by using ϕ_n and ψ_n via FFT. Once the problem is solved on the boundary of the scatter, at any point (inside or outside the object), the scattered field and its normal derivative can be computed by using the left-hand sides of (18) and (19).

Similar to the free space case, since the above operations involve the FFT of smooth functions, the accuracy of E_z and $\partial E_z/\partial n'$ increases exponentially as the number of the discrete points increases, a basic property of the FFT algorithm. For the layered medium case, however, the accuracy also depends on the accuracy of the layered medium Green's functions. Here, they are calculated adaptively, hence error-controllable to high accuracy.

In this work, the biconjugate-gradient (BCG) method is used to solve the matrix equation which requires $O(KN^2)$ CPU time and $O(N^2)$ memory, where N is the number of unknowns and K is the number of iterations. Since the main purpose of this work is the reduction of the number of unknowns (N), we have not implemented any acceleration methods (such as the fast multipole method and adaptive integral method) to further reduce the computation time and storage requirements.

IV. Numerical Results

A. A Circular Cylinder in Air

To show the accuracy and efficiency of the method, a circular dielectric object in free space is chosen as the first example as it has an analytical solution. An infinite dielectric circular cylinder with radius $r = 0.04$ m and $\epsilon_r = 16$ is excited with a TM_z plane wave at $f = 300$ MHz impinging at an angle $\theta^{\text{inc}} = 0^\circ$ along the x-direction. The receiver points are chosen along the $y = 1$ m line, from $x = -1$ m to $x = 1$ m. Fig. 2 shows the comparison between the SIM result and analytical solution for the scattered field. For this example, 64 points along the boundary of the object are used, and excellent agreement has been observed.

Fig. 3 shows the error convergence curve and the CPU time versus the number of discretization points per wavelength (PPW) on the dielectric object. The error decreases exponentially with the number of discretization points, confirming that the SIM has a spectral accuracy. The result shows that even with a small discretization number $N = 32$ (or at 2.7 PPW) on the boundary of the cylinder, the relative error is smaller than 1%.

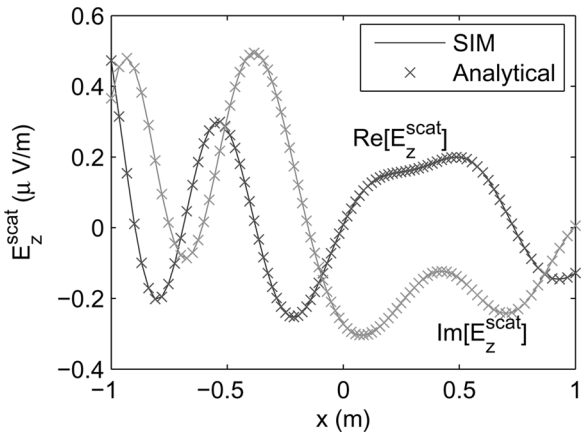

Fig. 2. *Example A*: Comparison of the SIM and analytical results for the real and imaginary parts of the scattered field for the free space case.

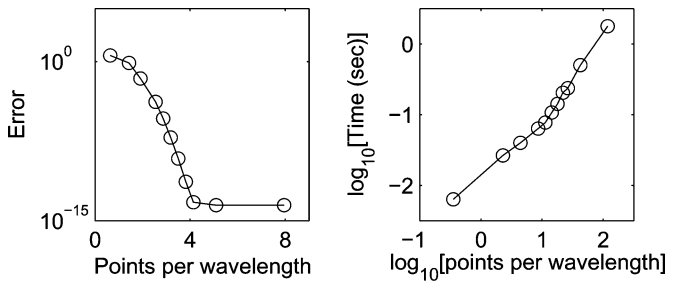

Fig. 3. Error and execution time versus the number of discretization points per wavelength for the free space case (*Example A*).

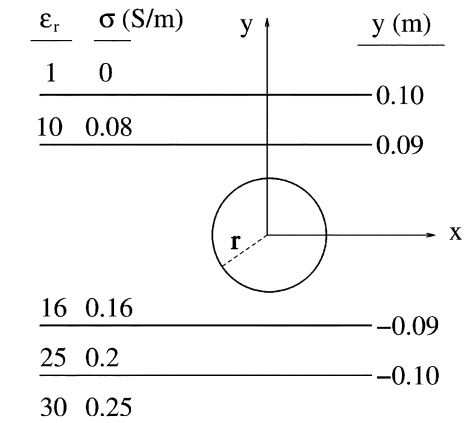

Fig. 4. *Example B*: Infinite circular dielectric cylinder embedded in a 5-layer medium.

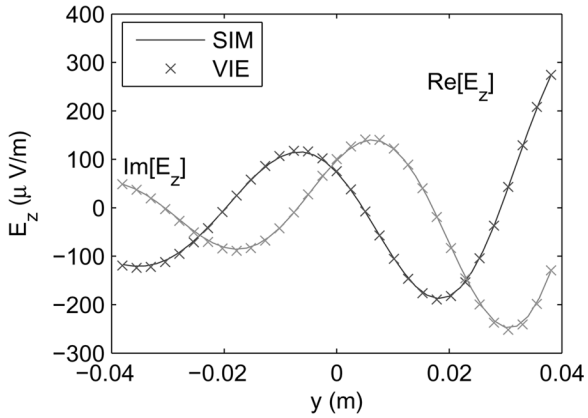

Fig. 5. Field E_z inside the scatterer along the (0.0:−0.04,0.04) m, for the circular dielectric object in a 5-layer medium in Fig. 4 (*Example B*).

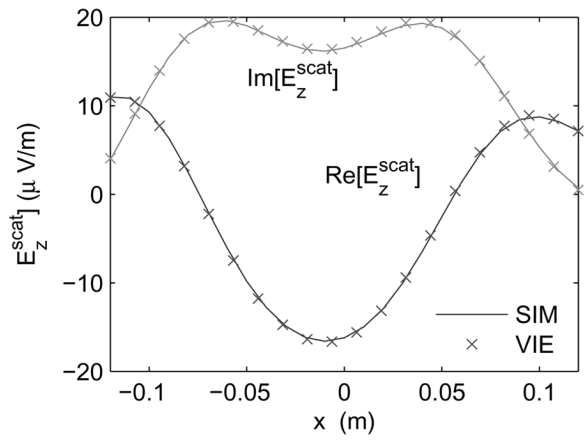

Fig. 6. Scattered field along the (−0.12:0.12,0.12) m for the circular dielectric object in a 5 layer medium in Fig. 4 (*Example B*).

B. A Circular Cylinder in a Five-Layer Medium

The second example is an infinite circular dielectric cylinder embedded in a 5-layer medium depicted in Fig. 4. All layers have different permittivity values and thickness. A line source is located at $(-0.12,\ 0.12)$ m, and the object with $r = 0.04$, $\epsilon_r = 57.2$, and $\sigma = 0.25\ \mathrm{S/m}$ is embedded in the third layer. Green's functions for the background have been calculated with a relative error tolerance of 10^{-8} relative. Fig. 5 shows the comparison of the field inside the object calculated with SIM and 2-D volume integral equation (VIE) approach [25], [26]. The test points are chosen along the $x = 0$ axis, from $y = -0.04$ m to $y = 0.04$ m. A very good agreement has been observed between the SIM and VIE results.

Fig. 6 compares the scattered field E_z^{scat} outside the object calculated with SIM and 2-D volume integral equation (VIE) approach [25], [26]. The test points are chosen along the $y = 0.12$ axis, from $x = -0.12$ m to $x = 0.12$ m. Excellent agreement is observed between the SIM and VIE results.

Another issue studied is the continuity of the scattered field across layer interfaces. Fig. 7 shows the comparison of scattered field along the $x = 0.06$ m axis, from $y = -0.12$ m to $y = 0.12$ m (from first layer to the last one). Both SIM and VIE results show expected continuity across layer interfaces.

The convergence of error with the number of discretization PPW is shown in Fig. 14. Since the Green's functions for the background have been calculated with 10^{-8} relative error tolerance, the minimum relative error that can be obtained is approximately in this level. Clearly, 2.7 PPW guarantees 1% accuracy.

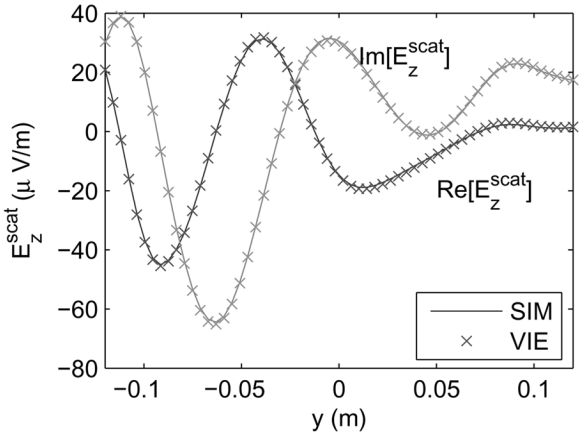

Fig. 7. Scattered field along the (0.06, −0.12:0.12) m for the circular dielectric object in a 5-layer medium in Fig. 4 (*Example B*).

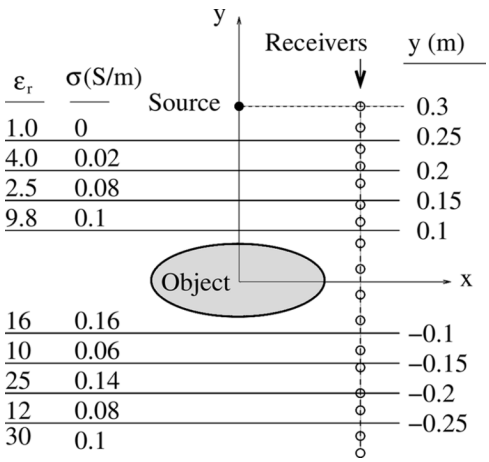

Fig. 8. Elliptical cylinder embedded in a 9-layer medium for *Example C*.

C. An Elliptical Dielectric Object in a Nine-Layer Medium

In the next example, an elliptical cylinder ($\epsilon_r = 57.2$ and $\sigma = 1.08\ \mathrm{S/m}$) is embedded in a 9-layer medium shown in Fig. 8. The elliptical object is defined as

$$x(\theta) = r_1 \cos(\theta) \quad y(\theta) = r_2 \sin(\theta)$$

where $r_1 = 0.08$ m, $r_2 = 0.04$ m, and $\theta \in (0, 2\pi)$.

A line source with $f = 400$ MHz is located at (0,0.3) m in the first layer. The receivers are located on $x = 0.12$ m axis from $y = 0.3$ m to $y = -0.3$ m (from top layer to the bottom layer). Fig. 9 shows the comparison of the real and imaginary parts of the scattered field obtained by using 16 points (4.16 PPW) and 128 points (33.27 PPW) on the object.

The convergence of error with the number of discretization PPW is obtained by using the case with 33.27 PPW as a reference and is shown in Fig. 14. Again, the minimum relative error that can be obtained is limited by the accuracy of the Green's functions for the background layered medium. Clearly, 4 PPW guarantees 1% accuracy.

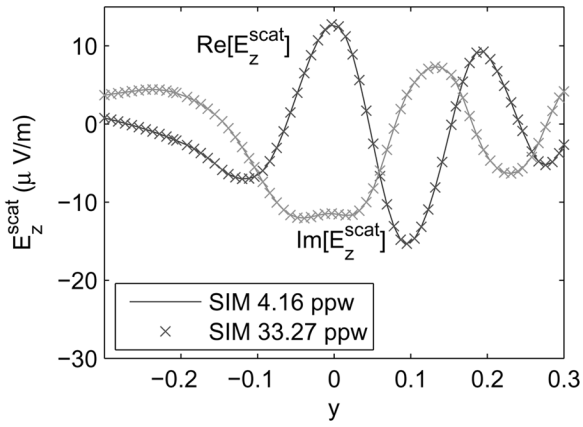

Fig. 9. *Example C*: Real and imaginary parts of the scattered field from the elliptical dielectric object in the 9-layer medium in Fig. 8.

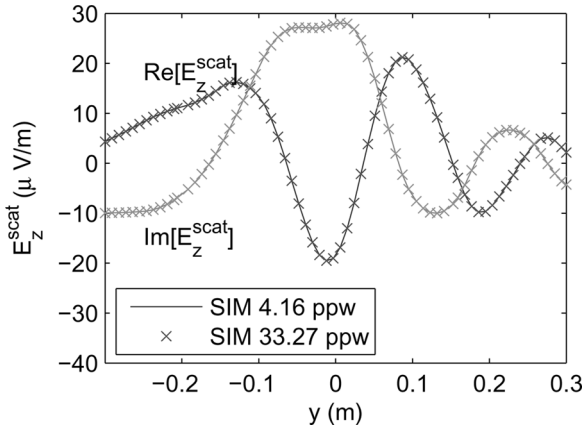

Fig. 10. *Example D*: Real and imaginary parts of the scattered field from the elliptical PEC object in the 9-layer medium in Fig. 8.

D. An Elliptical PEC Object in a Nine-Layer Medium

The fourth example is similar to the ones presented in [27] to demonstrate the validity of the method for PEC objects. Since the tangential component of the electric field is zero on the boundary, the integrals in (18) and (19) only have the first terms. In this case, a PEC object with the same elliptical shape as in the previous example is embedded in the 9-layer medium depicted in Fig. 8. All other properties are the same as in the previous case. Fig. 10 compares the scattered field obtained by using 12 points (4.3 PPW) and 128 points (45.9 PPW) on the object. The convergence of error with the number of discretization PPW is obtained by using the case with 45.9 PPW as a reference and is plotted as *Example D* in Fig. 14. Note that 1% accuracy can be obtained with 2.7 PPW sampling.

E. A Complex Object in a Nine-Layer Medium

A complex cylinder ($\epsilon_r = 57.2$, $\sigma = 1.08\ \mathrm{S/m}$) shown in Fig. 11 (left panel) is embedded at center of the 9-layer medium in Fig. 8. The object is defined as follows:

$$x(\theta) = 0.04\cos(\theta) + 0.006\sin(2\theta) + 0.0032625\cos(4\theta)$$
$$y(\theta) = 0.04\sin(\theta) + 0.006\cos(2\theta) + 0.0032625\sin(4\theta)$$

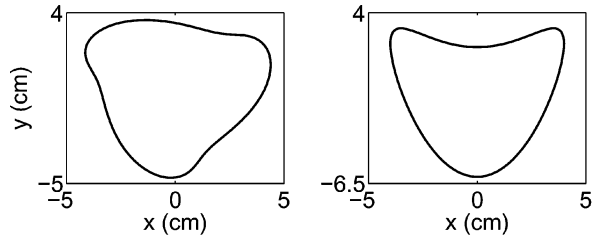

Fig. 11. Complex convex cylinder (left panel) for *Example E*, and a concave cylinder (right panel) for *Example F*.

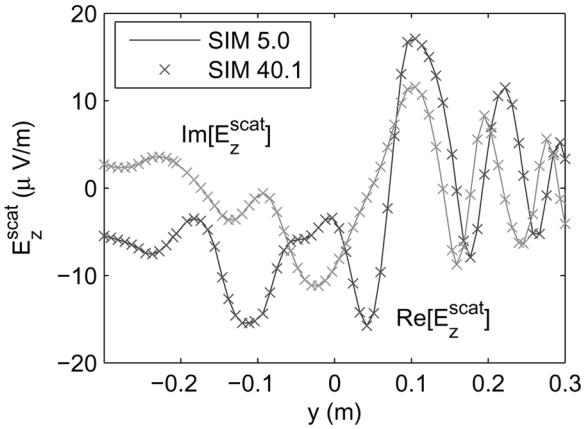

Fig. 12. *Example E*: Real and imaginary parts of the scattered field for a complex object shown in the left panel of Fig. 11 in the nine-layer medium in Fig. 8.

where $\theta \in (0, 2\pi)$. The frequency is 1 GHz and the circumference of the object is equal to $6.4\lambda_{\text{object}}$. A line source is located at (0,0.12) m. The receivers are located on $x = 0.2$ m axis from $y = 0.3$ m to $y = -0.3$ m (from top layer to the bottom layer). Fig. 12 shows the comparison of the real and imaginary parts of the scattered field obtained by using 32 points (5.0 PPW) and 256 points (40.1 PPW) on the object.

The convergence of error with the number of discretization PPW is obtained by using the case with 40.1 PPW as a reference and is shown in Fig. 14. Again, 2.7 PPW guarantees 1% accuracy.

F. A Concave Object in a Five-Layer Medium

In order to study the performance of the SIM for concave objects, we replace the circular object in *Example B* with a concave cylinder defined by $x(\theta) = 0.04\cos(\theta)$ and $y(\theta) = 0.04\sin(\theta) + 0.02\cos(2\theta)$ and shown in the right panel of Fig. 11. All other parameters are the same as in *Example B*. Fig. 13 shows the comparison of the real and imaginary parts of the scattered electric field along the (0.06, −0.12: 0.12) m obtained by using 24 points (4.6 PPW) and 256 points (49.0 PPW) on the object. The convergence of error with the number of discretization PPW is obtained by using the case with 49.0 PPW as a reference and is shown in Fig. 14.

In this work, we have used θ for parameterization of the object surface; alternatively, one can directly use the arc length for parameterization.

All the above examples demonstrate that the method has spectral accuracy for smooth objects. For the objects with corners, the method will be still valid but the expected accuracy will decrease from the smooth objects. Future studies will investigate non-smooth objects.

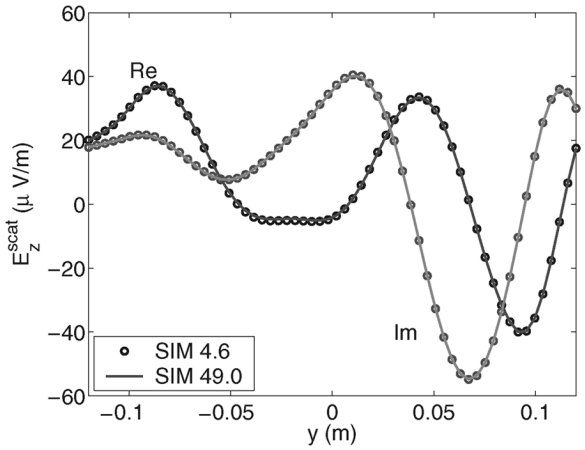

Fig. 13. *Example F*: real and imaginary parts of the scattered electric field along (0.06, −0.12: 0.12) m for a concave object in the right panel of Fig. 11 in a 5-layer medium in Fig. 4.

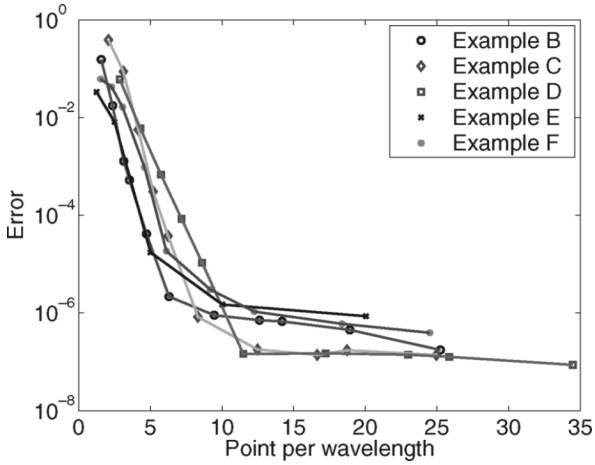

Fig. 14. Convergence of error with the number of discretization points for examples B through F.

V. Conclusion

We develop a spectral integral method for homogeneous dielectric objects and perfect conductors with closed smooth boundary embedded in a layered medium. The high accuracy and the efficiency of the method has been demonstrated. 1% accuracy can be obtained with about three points per wavelength sampling. Numerical results also confirm that the SIM is applicable to concave objects. The method can be further extended to periodic structures and to three dimensions, as well as to objects traversing layer interfaces.

Acknowledgment

The authors thank the anonymous reviewers for their constructive comments that greatly improve the manuscript.

References

[1] K. A. Michalski and D. Zheng, "Electromagnetic scattering and radiation by surfaces of arbitrary shape in layered media: part I: theory," *IEEE Trans. Antennas Propag.*, vol. 38, pp. 335–344, Mar. 1990.

[2] ——, "Electromagnetic scattering and radiation by surfaces of arbitrary shape in layered media: part II: Implementation and results for contiguous half-spaces," *IEEE Trans. Antennas Propag.*, vol. 38, pp. 355–352, Mar. 1990.
[3] N. Geng and L. Carin, "Wide-band electromagnetic scattering from a dielectric BOR buried in a layered lossy dispersive medium," *IEEE Trans. Antennas Propag.*, vol. 47, pp. 610–619, Apr. 1999.
[4] Y. Liu, L. W. Li, T. S. Yeo, and M. S. Leong, "Application of DCIM to MPIE-MoM analysis of 3-D PEC objects in multilayered media," *IEEE Trans. Antennas Propag.*, vol. 50, pp. 157–162, Feb. 2002.
[5] E. Jørgensen, O. S. Kim, P. Meincke, and O. Breinbjerg, "Higher order hierarchical discretization scheme for surface integral equations for layered media," *IEEE Trans. Geosci. Remote Sensing*, vol. 42, no. 4, pp. 764–772, Apr. 2004.
[6] Y. H. Chen, W. C. Chew, and S. Zeroug, "Fast multipole method as an efficient solver for 2-D elastic wave surface integral equations," *Computat. Mechan.*, vol. 20, no. 6, pp. 495–506, Nov. 1997.
[7] B. Hu and W. C. Chew, "Fast inhomogeneous plane wave algorithm for electromagnetic solutions in layered medium structures: 2-D case," *Radio Sci.*, vol. 35, no. 1, pp. 31–43, 2000.
[8] ——, "Fast inhomogeneous plane wave algorithm for scattering from objects above the multilayered medium," *IEEE Trans. Geosci. Remote Sens.*, vol. 39, no. 5, pp. 1028–1038, 2001.
[9] N. Geng, A. Sullivan, and L. Carin, "Multilevel fast-multipole algorithm for scattering from conducting targets above or embedded in a lossy half space," *IEEE Trans. Geosci. Remote Sens.*, vol. 38, pp. 1561–1573, Jul. 2000.
[10] ——, "Fast multipole method for scattering from an arbitrary PEC target above or buried in a lossy half space," *IEEE Trans. Antennas Propag.*, vol. 49, pp. 740–748, May 2001.
[11] E. Bleszynski, M. Bleszynski, and T. Jaroszewicz, "A fast integral equation solver for electromagnetic scattering problems," in *IEEE AP-S Int. Symp. Dig.*, Seattle, WA, Jun. 1994, pp. 416–419.
[12] ——, "AIM: Adaptive integral method for solving large-scale electromagnetic scattering and radiation problems," *Radio Sci.*, vol. 31, no. 5, pp. 1225–1252, 1996.
[13] F. Ling, C. F. Wang, and J. M. Jin, "Application of adaptive integral method to scattering and radiation analysis of arbitrarily shaped planar structures," in *IEEE Antennas and Propagat. Soc. Int. Symp.*, Jun. 1998, vol. 3, pp. 1778–1781.
[14] S. S. Bindiganavale, J. L. Volakis, and H. Anastassiu, "Scattering from planar structures containing small features using the adaptive integral method (AIM)," *IEEE Trans. Antennas Propag.*, vol. 46, no. 12, pp. 1867–1878, 1998.
[15] E. Topsakal, M. Carr, J. L. Volakis, and M. Bleszynski, "Scattering from 3-D multi-layered surfaces using adaptive integral method," in *IEEE Antennas and Propag. Soc. Int. Symp.*, Jul. 2000, vol. 4, pp. 1868–1871.
[16] A. E. Yilmaz, J. M. Jin, and E. Michielssen, "Time domain adaptive integral method for surface integral equations," *IEEE Trans. Antennas and Propagation*, vol. 52, no. 10, pp. 2692–2708, Oct. 2004.
[17] J. Liu and Q. H. Liu, "A Spectral Integral Method (SIM) for periodic and nonperiodic structures," *IEEE Microwave Wireless Comp. Lett.*, vol. 13, pp. 97–99, Mar. 2004.
[18] N. N. Bojarski, "Scattering by a cylinder: A fast exact numerical solution," *J. Acoust. Soc. Amer.*, vol. 75, no. 2, pp. 320–323, 1984.
[19] G. T. Schuster, "A fast exact numerical solution for the acoustic response of concentric cylinders with penetrable interfaces," *J. Acoust. Soc. Amer.*, vol. 87, no. 2, pp. 495–502, 1990.
[20] F. Q. Hu, "A spectral boundary integral equation method for the 2-D Helmholtz equation," *J. Comp. Phys.*, vol. 120, pp. 340–347, 1995.
[21] W. C. Chew, *Waves and Fields in Inhomogeneous Media*. Piscataway, NJ: IEEE Press, 1995.
[22] K. A. Michalski and J. R. Mosig, "Multilayered media Green's functions in integral equation formulations," *IEEE Trans. Antennas Propag.*, vol. 45, pp. 508–519, Mar. 1997.
[23] M. Paulus, P. Gay-Balmaz, and O. J. F. Martin, "Accurate and efficient computation of the Green's tensor for stratified media," *Phys.Rev.*, vol. 62, no. 4, pp. 5797–5807, Oct. 2000.
[24] E. Simsek, Q. H. Liu, and B. Wei, "Singularity subtraction for evaluation of Green's functions for multilayer media," *IEEE Trans. Microwave Theory Tech.*, vol. 54, no. 1, pp. 216–225, Jan. 2006.
[25] X. Millard and Q. H. Liu, "A fast volume integral equation solver for electromagnetic scattering from large inhomogeneous objects in planarly layered media," *IEEE Trans. Antennas Propag.*, vol. 51, no. 9, pp. 2393–2401, 2003.
[26] L. P. Song, E. Simsek, and Q. H. Liu, "A fast 2-D volume integral equation solver for scattering from inhomogeneous objects in layered media," *Microwave Opt. Technol. Lett.*, vol. 47, no. 2, pp. 128–134, 2005.
[27] E. Simsek and Q. H. Liu, "Fast computation of dyadic Green's function for layered media and its application in interconnect simulations," in *Proc. USNC/URSI Nat. Radio Science Meeting*, Monterey, CA, Jun. 20–25, 2004, vol. 3, p. 2783.
[28] L. B. Felsen and A. H. Kamel, "Hybrid ray-mode formulation of parallel plane waveguide Green's functions," *IEEE Trans. Antennas Propagat.*, vol. AP-29, pp. 637–649, Jul. 1981.
[29] M. I. Aksun, "A robust approach for the derivation of closed-form Green's functions," *IEEE Trans. Microwave Theory Tech.*, vol. MTT-44, pp. 651–658, May 1996.

Ergün Şimşek (S'01) received the B.A. degree in electrical engineering from Bilkent University, Ankara, Turkey, in 2001 and the M.S. degree in electrical and computer engineering from the University of Massachusetts at Dartmouth, in 2003.

He is currently working toward the Ph.D. degree at Duke University, Durham, NC, where he has been a Research Assistant since 2003. His research interests include numerical methods and computational electromagnetics.

Jianguo Liu (S'05) received the B.S. degree in physics from Northeast Normal University, Changchun, China, in 1995 and the M.E. degree in underwater acoustics engineering from Harbin Engineering University, Harbin, China, in 1998.

From 1998 to 2003, he worked at the Institute of Acoustics, Chinese Academy of Sciences. He is currently working toward the Ph.D. degree at Duke University, Durham, NC where he has been a Research Assistant since 2003. His research interests are computational acoustics, experimental underwater sound propagation and computational electromagnetics.

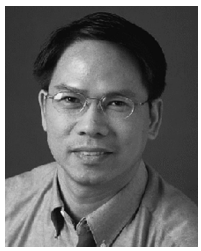

Qing Huo Liu (S'88–M'89–SM'94–F'05) received the Ph.D. degree in electrical engineering from the University of Illinois at Urbana-Champaign, in 1989.

He was with the Electromagnetics Laboratory at the University of Illinois at Urbana-Champaign as a Research Assistant from September 1986 to December 1988, and as a Postdoctoral Research Associate from January 1989 to February 1990. He was a Research Scientist and Program Leader with Schlumberger-Doll Research, Ridgefield, CT, from 1990 to 1995. From 1996 to May 1999, he was an Associate Professor with New Mexico State University. Since June 1999, he has been with Duke University where he is now a Professor of electrical and computer engineering. He has published more than 300 papers in refereed journals and conference proceedings. His research interests include computational electromagnetics and acoustics, inverse problems, geophysical subsurface sensing, biomedical imaging, electronic packaging, and the simulation of photonic and nano devices.

Dr. Liu is a Fellow of the Acoustical Society of America, a member of Phi Kappa Phi, Tau Beta Pi, and a full member of the U.S. National Committee of URSI Commissions B and F. Currently he serves as an Associate Editor for *Radio Science* and the IEEE TRANSACTIONS ON GEOSCIENCE AND REMOTE SENSING, for which he also served as a Guest Editor for a Special Issue on Computational Methods. He received the 1996 Presidential Early Career Award for Scientists and Engineers (PECASE) from the White House, the 1996 Early Career Research Award from the Environmental Protection Agency, and the 1997 CAREER Award from the National Science Foundation.